1   Differential protein phosphorylation affects the localisation of two secreted *Toxoplasma*

2   proteins and is widespread during stage conversion.

3

4   Running title: Phosphorylation in *Toxoplasma* stage conversion

5   Joanna Young[a], Malgorzata Broncel[a,e], Helena Teague[a*], Matt Russell[b], Olivia McGovern[c$], Matt

6   Renshaw[d], David Frith[e], Bram Snijders[e], Lucy Collinson[b], Vern Carruthers[c], Sarah Ewald[f], Moritz

7   Treeck[a#]

8

9   [a] Signalling in Apicomplexan Parasites Laboratory, The Francis Crick Institute, London, UK

10   [b] Electron Microscopy Science Technology Platform, The Francis Crick Institute, London, UK

11   [c] Department of Microbiology and Immunology, University of Michigan Medical School, Ann

12   Arbor, Michigan, USA

13   [d] Advanced Light Microscopy Science Technology Platform, The Francis Crick Institute, London,

14   UK

15   [e] Proteomics Science Technology Platform, The Francis Crick Institute, London, UK

16   [f] Department of Microbiology, Immunology and Cancer Biology and the Carter Immunology

17   Center, University of Virginia, Charlottesville , Virginia, USA

18   #correspondance to: Moritz.treeck@crick.ac.uk

19   *Present address: Department of Pathology, University of Cambridge, UK

20   [$] Present address: Epidemic Intelligence Service, Respiratory Diseases Branch, Centers for

21   Disease Control and Prevention, Atlanta,USA

23   ABSTRACT

24   The intracellular parasite *Toxoplasma gondii* resides within a membrane bound

25   parasitophorous vacuole (PV) and secretes an array of proteins to establish this replicative

26   niche. It has been shown previously that *Toxoplasma* both secretes kinases and that numerous

27   proteins are phosphorylated after secretion. Here we assess the role of phosphorylation of

28   SFP1 and the related GRA29, two secreted proteins with unknown function. We show that both

29   proteins form stranded structures in the PV that are independent of the previously described

30   intravacuolar network or actin. GRA29 likely acts as a seed for SFP1 strand formation, and these

31   structures can form independently of other *Toxoplasma* secreted proteins. We show that an

32   unstructured region at the C-terminus of SFP1 and GRA29 is required for the formation of

33   strands and that mimicking phosphorylation of this domain negatively regulates strand

34   development. When tachyzoites convert to chronic stage bradyzoites, both proteins show a

35   dispersed localisation throughout the cyst matrix. Many secreted proteins are reported to

36   dynamically redistribute as the cyst forms and secreted kinases are known to play a role in cyst

37   formation. Using quantitative phosphoproteome and proteome analysis comparing tachyzoite

38   and early bradyzoite stages, we reveal widespread differential phosphorylation of secreted

39   proteins. These data support a model in which secreted kinases and phosphatases are

40   important to dynamically regulate parasite secreted proteins during stage conversion.

41   IMPORTANCE

42   *Toxoplasma gondii* is a common parasite that infects up to one third of the human population.

43   Initially the parasite grows rapidly, infecting and destroying cells of the host, but subsequently

44   switches to a slow-growing form and establishes chronic infection. In both stages the parasite

45   lives within a membrane bound vacuole within the host cell, but in the chronic stage a durable

46   cyst wall is synthesized that provides protection to the parasite during transmission to a new

47   host. *Toxoplasma* secretes proteins into the vacuole to build its replicative niche and previous

48   studies identified many of these proteins as phosphorylated. We investigate two secreted

49   proteins and show that phosphorylation plays an important role in their regulation. We also

50   observed widespread phosphorylation of secreted proteins when parasites convert from acute

51   to chronic stages, providing new insight into how the cyst wall may be dynamically regulated.

52   **INTRODUCTION**

53   The apicomplexan parasite *Toxoplasma gondii* is widespread infecting approximately one third

54   of the world's population (1). Although *Toxoplasma* infection is predominantly asymptomatic

55   in healthy hosts, complications occur in the immunocompromised, such as cancer and HIV

56   patients, and in pregnant women. In these patients, infection can cause encephalitis, or

57   severely damage the unborn foetus during pregnancy (2). Additionally, *Toxoplasma* is a leading

58   cause of retinocharditis (3), and an expansion of strain diversity in South America is causing

59   substantial ocular disease (4).

60   *Toxoplasma* actively invades nucleated cells of virtually any warm-blooded animal and

61   subsequently replicates within a membrane-bound parasitophorous vacuole (PV). During the

62   acute stage of infection, the rapidly growing tachyzoites complete rounds of invasion and lysis

63   of host cells and disseminate around the body. Upon immune pressure or other stress, the

64   parasite converts to slow-growing bradyzoites that form cysts, predominantly in skeletal

65   muscle and the brain (5). The cyst is a modified PV with a protective cyst wall that allows the

66   parasite to establish chronic, perhaps lifelong infection of the host.

67 During infection *Toxoplasma* secretes proteins that subvert host cell signalling and develops its

68 replicative niche within the PV (6, 7). The repertoire of secreted proteins is thought to include

69 up to 200 proteins (ToxoDB, LOPIT dataset) including 50 kinases/pseudokinases (8), although

70 the functions of many of these remain unknown. These proteins are secreted from the

71 rhoptries or dense granules and are called ROPs or GRAs, respectively. Secreted proteins

72 extensively modify the PV allowing selective passage of molecules and proteins across the PV

73 membrane. For example, GRA17 and GRA23 form pores in the PV membrane allowing the

74 passage of small molecules into the PV (9), while the MYR complex mediates the transport of

75 secreted proteins to the host cell (10, 11). Additionally, the parasite develops a complex set of

76 membrane structures within the PV including GRA7-lined invaginations (12) and a network of

77 tubules called the intravacuolar network (IVN) (13). The formation of this network is dependent

78 on GRA2 and the accessory protein GRA6, and is required for full virulence in mice (14, 15).

79 Both structures have been reported to play a role in scavenging nutrients from the host cell

80 with the uptake of host cell proteins (16), lipid droplets (17), and endolysosomal compartments

81 (18).

82 Previous phosphoproteome analysis revealed that a large number of *Toxoplasma* secreted

83 proteins are phosphorylated after their release (19), raising the intriguing possibility that their

84 function is dynamically regulated. Indeed, the PV localised kinase WNG1 was shown to

85 contribute to formation of a functional IVN (20). Furthermore, it was recently shown that IVN

86 associated GRAs show dynamic localisation patterns as the parasite remodels the PV to form

87 the chronic stage cyst (21). Here we analyse two secreted, strand forming proteins that are

88 phosphorylated after secretion and show that phosphorylation regulates their localisation,

89 disrupting normal strand formation. Both proteins disperse in chronic stage cysts, so we

90   expand the analysis to compare the phosphoproteome of acute and chronic stage parasites.

91   We show that many GRAs are differentially phosphorylated between these stages, suggesting

92   that phosphorylation of secreted proteins may be a key determinant for dynamic restructuring

93   of the replicative niche of *Toxoplasma*.

94   **RESULTS**

95   **A secreted protein forms strand-like structures in the parasitophorous vacuole independently**

96   **of the intravacuolar network and actin.**

97   To investigate the role of phosphorylation of secreted proteins we selected TGGT1_289540 as

98   an ideal candidate. It is substantially phosphorylated after secretion (19) and contains a

99   localised cluster of phosphorylation sites in its C-terminus, allowing for targeted genetic

100   mutagenesis. TGGT1_289540 contains a signal peptide, four coiled-coil domains and an

101   unstructured C-terminus which contains 8 phosphorylation sites (Fig. 1A). Three further

102   phosphorylation sites are located within the rest of the protein. To first verify that

103   TGGT1_289540 is a secreted protein, we expressed a myc-tagged version of the protein which

104   localised to the PV. Interestingly, in contrast to most GRAs that are either found to fill the space

105   between parasites, or are found associated with the PV membrane, TGGT1_289540 appeared

106   in strand- or filament-like structures (Fig.1B). Western-blotting confirmed the presence of a

107   single isoform of myc-tagged protein at the predicted size of ~100kDa in transgenic parasites,

108   but not in a WT control (Fig. 1C).

109   To verify this unusual distribution of TGGT1_289540 in the PV, we generated polyclonal

110   antibodies against the recombinant protein. The antibody recognised a band in Western blot

111   that was absent in WB and IFA when the *TGGT1_289540* locus was disrupted (Fig. 1D,E). As

5

112
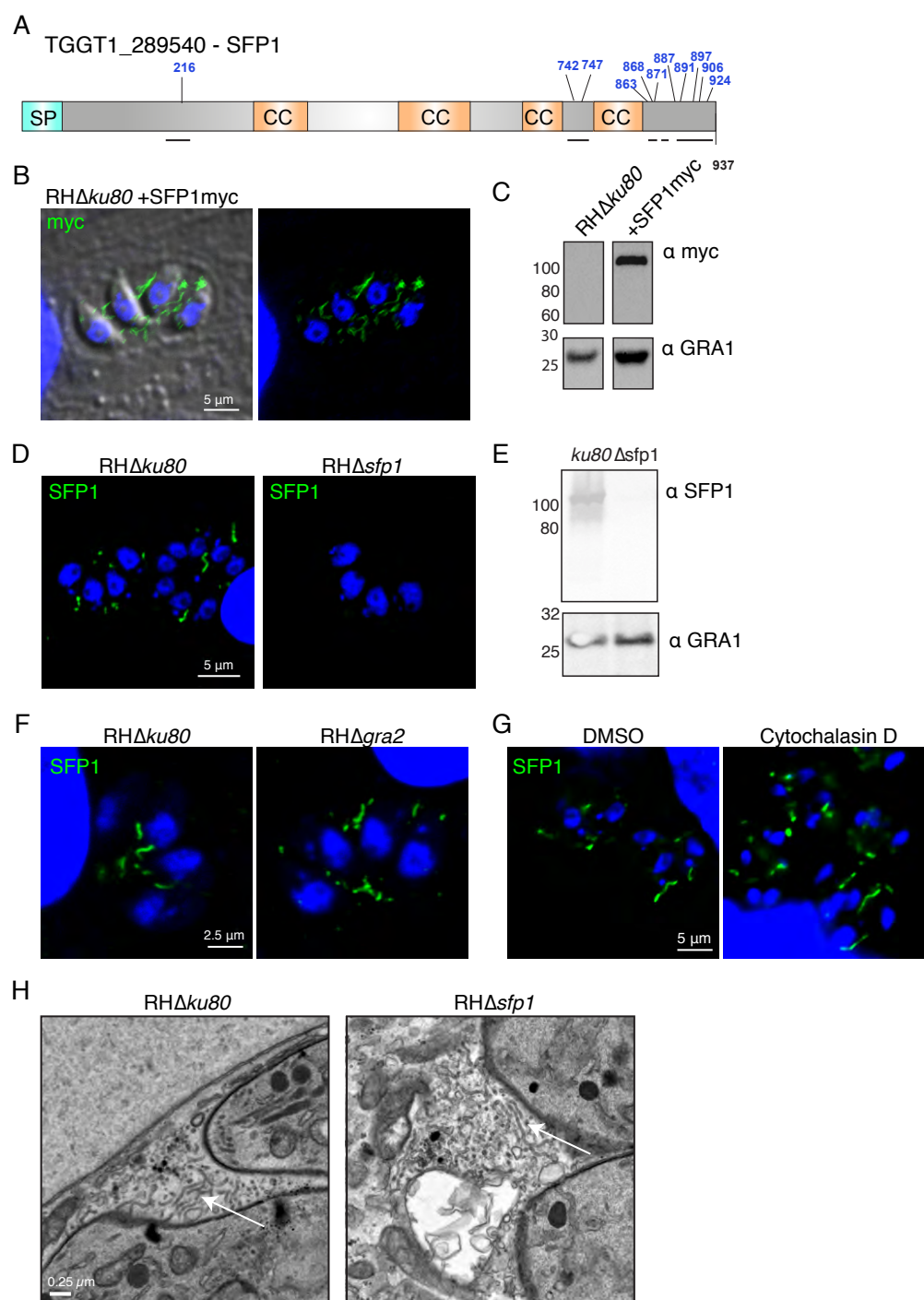
Figure 1. SFP1 forms strands in the parasitophorous vacuole that are distinct from the intravacuolar network. a) Schematic of TGGT1_289540 (SFP1) indicating predicted domains and previously identified phosphosites (shown in blue). Signal peptide (SP), coiled coil (CC). Black lines show predicted unstructured regions. b) Immunofluorescence images of HFFs infected with RHΔku80 parasites expressing SFP1-myc. Anti-myc antibody (green) and DAPI (blue). c) Western blot of immunoprecipitated TGGT1_289540::myc. Anti-GRA1 antibodies were used to probe the non-bounds fraction as a loading control. d) Immunofluorescence images of HFFs infected with RHΔku80 and RHΔsfp1 parasites. Polyclonal anti-SFP1 antibodies

121   (green) and DAPI (blue). **e)** Western blot analysis of lysates from HFFs infected with RHΔ*ku80*

122   and RHΔ*sfp1* parasites probed with anti-SFP1 and anti-GRA1 antibodies. **f)** SFP1 strands do not

123   depend on GRA2 and the IVN. Immunofluorescence analysis of RHΔ*ku80* and RHΔ*gra2* infected

124   HFFs. Anti-SFP1 antibodies (green) and DAPI (blue). **g)** SFP1 strands do not depend on actin

125   filamentation. Immunofluorescence analysis of infected HFFs treated with 1uM Cytochalasin D

126   or DMSO control. Anti-SFP1 antibody (green) and DAPI (blue). **h)** SFP1 is not required for IVN

127   formation. Electron micrographs of HFFs infected with RHΔ*ku80* and RHΔ*sfp1* for 16 h.

128   Examples of Intravacuolar network tubules are indicated by arrows.

129   was the case with the myc-tagged isoform, analysis of the endogenous protein showed a

130   filamentous distribution in the PV (Fig. 1D).

131   As the *Toxoplasma* PV contains a distinct IVN of membranous tubules we tested whether the

132   strands were related to these structures. The formation of the IVN is dependent on GRA2 so

133   we assessed TGGT1_289540 localisation in RHΔ*gra2* parasites that lack the IVN (14). No

134   obvious difference in filamentous TGGT1_289540 localisation was observed (Fig. 1F),

135   indicating that the filaments are distinct from, and their formation does not depend on the

136   IVN. We therefore named the protein Strand Forming Protein 1 (SFP1 hereafter).

137   We hypothesised that SFP1 strands could function in transport between the parasites and the

138   host cell. *Toxoplasma* endocytoses proteins from the host cell through an unknown mechanism

139   (16) so we assessed whether SFP1 plays a role in the uptake of proteins from the host cell into

140   the parasite at 3h post infection. As endocytosed material is rapidly digested, this can only be

141   observed upon inhibition of cathepsin protease L function with the inhibitor morpholinurea-

142   leucine-homophenylalanine-vinyl phenyl sulphone (LHVS)(16). Under these conditions there

143   was no difference in the proportion of parasites that had taken up Venus fluorescent protein

144   from the host cell indicating SFP1 does not contribute to protein uptake (Fig. S1A). *Toxoplasma*

145   upregulates host c-Myc in infected cells, a phenotype that is dependent on protein

146   translocation from the PV into the host cell (10, 22). To test whether SFP1 plays a role in protein

7

147   export into the host cell we compared the ability of wild type and Δ*sfp1* parasites to upregulate

148   host c-Myc. No differences where observed in host cell c-Myc upregulation, indicating that

149   SFP1 does not play a role in protein export from the PV (Fig. S1B).

150   It was recently shown that long filaments of actin extend into the PV during *Toxoplasma*

151   infection (23). We therefore tested whether treatment with cytochalasin D, to depolymerise

152   actin, would disrupt SFP1 strand formation. We still saw substantial filamentation of SFP1 in

153   the presence of cytochalasin D, indicating that actin is not important in this process (Fig. 1G).

154   While the presence of the IVN is not important for SFP1 filament formation, the opposite could

155   be true, that is, that SFP1 may be important for the formation of the IVN. However, IVN

156   formation was not affected in the absence of SFP1 as shown by transmission electron

157   microscopy (Fig. 1H). No obvious abnormalities in the overall PV organisation or PVM structure

158   were observed in RHΔ*sfp1* parasites.

159   Collectively these data indicate that SFP1, a protein that was reported to be phosphorylated

160   after secretion, localises to the PV, and forms novel, IVN- and actin-independent filamentous

161   structures. These, as suggested by our data, do not contribute to protein uptake from, or

162   protein export into the host cell.

163   **A second SFP1 related protein, GRA29, forms related structures**

164   As secreted protein families can form by gene duplication and diversification, we looked for

165   potential paralogs of SFP1 in the *Toxoplasma* genome using BlastP. We identified a single

166   protein (TGGT1_269690, GRA29) with 24 % identity and a similar architecture (Fig. 2A & S2) of
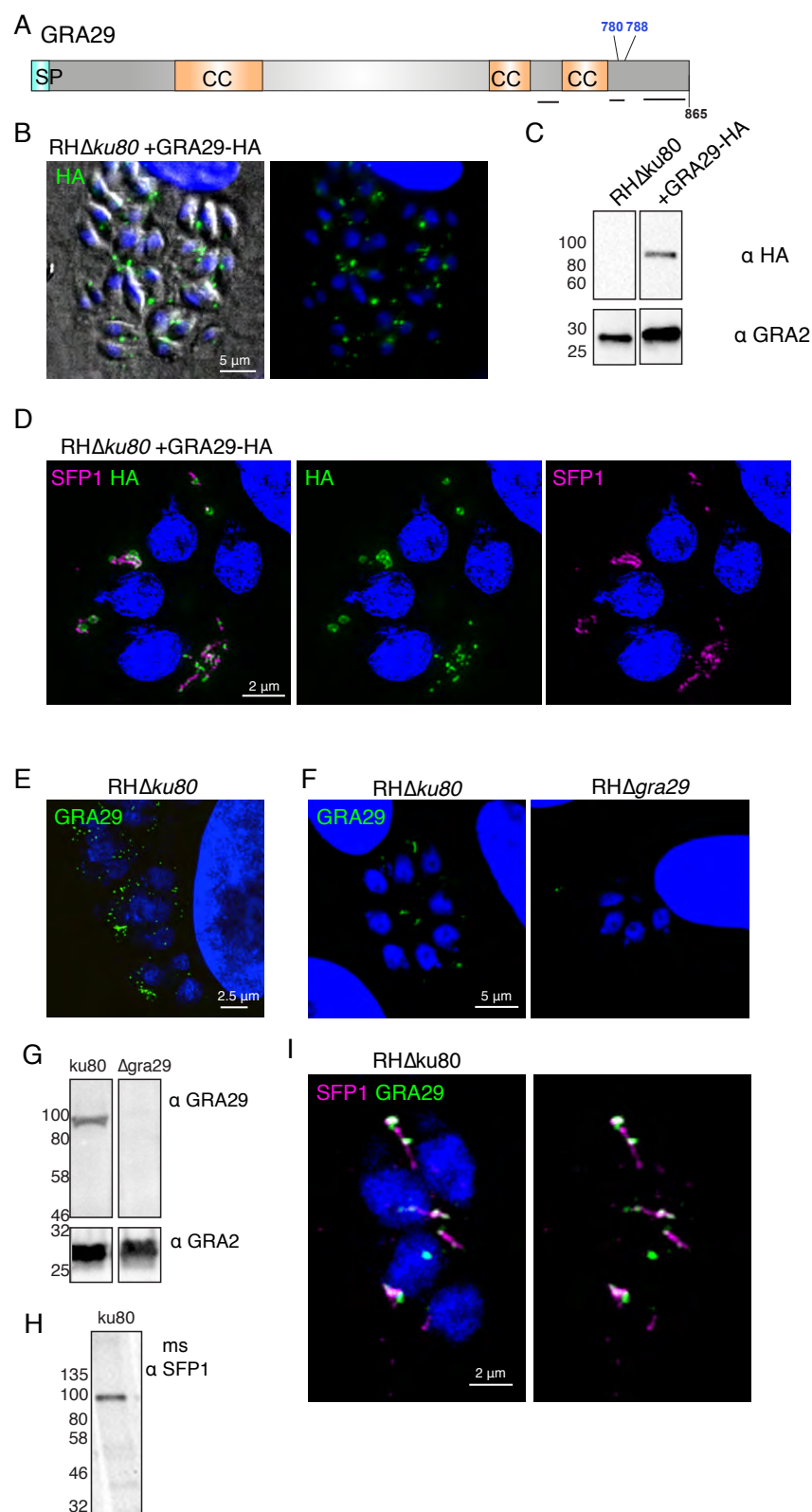
Figure 2. GRA29 shares homology with SFP1 and forms similar structures in the PV. a) Schematic of GRA29 indicating predicted domains and previously identified phosphosites (shown in blue). Signal peptide (SP), coiled coil (CC). Black lines show predicted unstructured regions. b) Immunofluorescence analysis of HFFs infected with RHΔ*ku80*::GRA29-HA. Anti-HA

9

172 antibodies (green) and DAPI (blue). **c)** Western blot analysis of RHΔ*ku80* or RHΔ*ku80*::GRA29-

173 HA infected HFFs with anti-HA and anti-GRA2 antibodies to verify expression of HA-tagged

174 protein. **d)** Structured Illumination microscopy (SIM) of HFFs infected with RHΔ*ku80*::GRA29-

175 HA. Anti-HA (green), anti-SFP1 (magenta) and DAPI (blue). **e)** SIM analysis of RHΔku80. Anti-

176 GRA29 antibodies (green) and DAPI (blue) **f)** Immunofluorescence analysis of HFFs infected

177 with RHΔ*ku80* and RHΔ*gra29* parasites. Anti-GRA29 (green) and DAPI (blue). **g)** Western blot

178 of RHΔ*ku80* and RHΔ*gra29* infected HFFs probed with anti-GRA29 and anti-GRA2 antibodies.

179 **h)** Western blot of RHΔ*ku80* infected HFFs probed with mouse anti-SFP1 antibodies generated

180 against SFP1 C-terminal showing a band of the expected size. **i)** SIM analysis of RHΔ*ku80*

181 infected HFFs. Mouse anti-SFP1 (magenta), anti-GRA29 (green) and DAPI (blue). See also Fig.

182 S3.

183 a signal peptide, coiled-coil domains and, like SFP1, C terminal phosphorylation sites that

184 appear phosphorylated after secretion (19). To compare localisation of this protein with that

185 of SFP1 we generated an HA-tagged version which by IFA localised to the PV and Western blot

186 showed an expected size of ~94 kDa (Fig. 2B,C). In contrast to SFP1 however, we saw smaller

187 filamentous structures and also large puncta associated with the parasites (Fig. 2B) consistent

188 with the localisation reported by Nadiparum *et al (24)*. To investigate whether SFP1 and GRA29

189 were within the same structures, we performed super-resolution microscopy using anti-SFP1

190 antibodies and anti-HA antibodies to localise GRA29. At this improved resolution GRA29 puncta

191 appeared as round spheres or doughnuts, often with SFP1 filaments associated or branching

192 out from them (Fig. 2D). We also observed filamentous SFP1 with smaller dots and strands of

193 GRA29. To further investigate these unusual sphere-like structures we performed correlative

194 light-electron microscopy (CLEM) to identify the subcellular structures. This revealed that

195 GRA29::HA accumulates in electron dense particles in the PV that appear to contain no

196 membrane and resembles proteinaceous aggregates (Figure S3).

197 To further investigate and verify GRA29::HA structures, we raised polyclonal antibodies against

198 recombinant GRA29. With the antibodies against endogenous protein we observed only short

199   strands and small puncta in the PV that did not resemble the HA-tagged parasite line (Fig. 2E,F).

200   The specificity of the antibodies was verified by Western blot and IFA, which showed the

201   expected molecular weight and positive IFA signal in WT, but not in GRA29 KO parasites (Fig.

202   2F,G). This indicates that the addition of the C-terminal HA tag disrupts GRA29 localisation,

203   inducing protein aggregates, suggesting a potentially important role of the C-terminal region.

204   In order to colocalise endogenous non-tagged SFP1 and GRA29 we generated antibodies

205   against SFP1 peptides in mice which showed the expected reactivity in IFA and Western blot

206   (Fig. 2H, I). Co-localisation of SFP1 and GRA29 revealed that both appear in similar structures,

207   with GRA29 often present at either end of SFP1 filaments (Fig. 2I).

208   Collectively these data show that SFP1 and GRA29 form novel filamentous structures in the PV.

209   C-terminal tagging of GRA29 alters its localisation, either causing or stabilising unusual

210   structures that SFP1 can still associate with.

211   **GRA29 initiates SFP1 strand formation, even in the absence of other *Toxoplasma* proteins**

212   As SFP1 and GRA29 appeared to localise within the same structures we hypothesised that they

213   may show an interdependence. To address this, we localised SFP1 in RHΔ*gra29,* and GRA29 in

214   RHΔ*sfp1* parasite lines using the specific antibodies raised. Whereas no alteration in GRA29

215   was observed in RHΔ*sfp1*, SFP1 formed fewer and longer filaments in the absence of GRA29

216   (Fig. 3A). To identify whether any other *Toxoplasma* proteins are required for i) SFP1 filament

217   formation and ii) SFP1 filament initiation, we expressed both SFP1 and GRA29, lacking their

218   respective signal peptides, in human foreskin fibroblasts (HFFs). Both, SFP1 and GRA29 formed

219   long filamentous structures in HFFs (Fig. 3B), often filling the complete cytoplasm, and in the

220   case of GRA29, sometimes associated with nucleus. Strikingly, when co-expressed in HFFs,

221   GRA29 frequently formed smaller puncta from which SFP1 filaments radiated suggesting

222   GRA29 can initiate SFP1 strand formation (Fig. 3C).
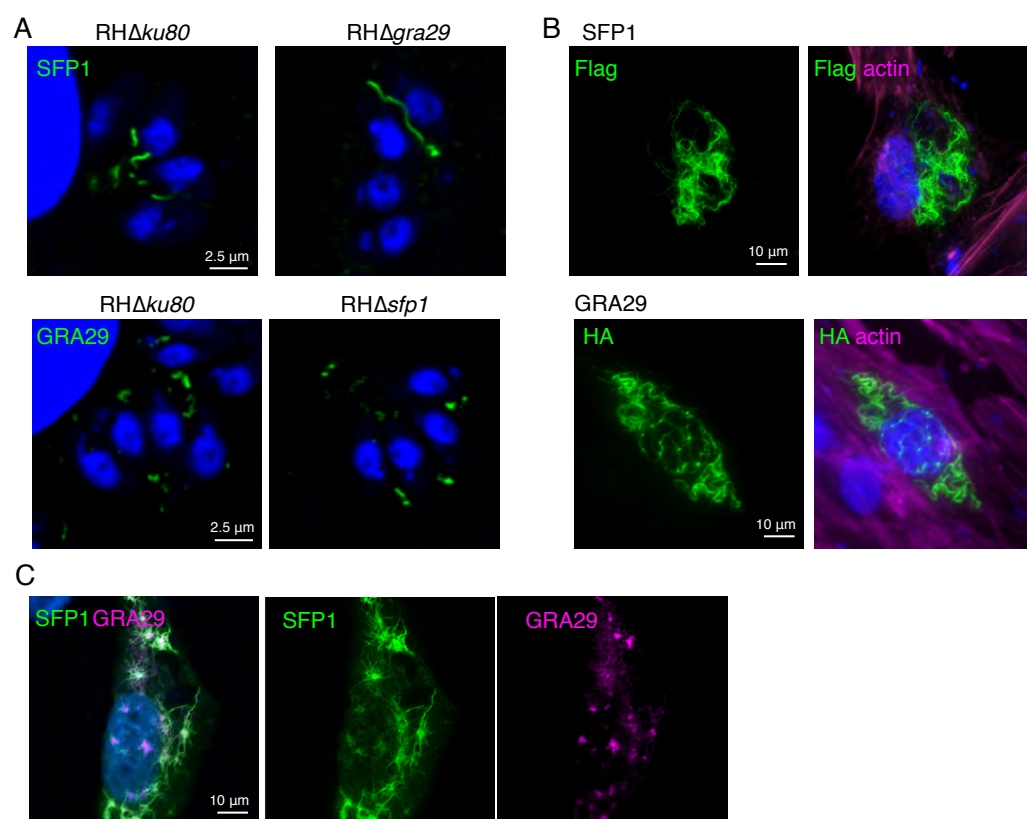
Figure 3. GRA29 regulates SFP1 strand formation. a) Fewer and longer SFP1 strands form in the absence of GRA29. Immunofluorescence analysis of HFFs infected with RHΔ*ku80*, RHΔ*sfp1* or RHΔ*gra29.* Anti-SFP1 (top panel), anti-GRA29 (lower panel) and DAPI (blue). **b)** SFP1 and GRA29 form strands when ectopically expressed. Immunofluorescence analysis of HFFs expressing N-terminally tagged SFP1 (Flag) or GRA29 (HA). Anti-Flag or HA antibodies (green), Phalloidin (magenta) to visualise F-actin, and DAPI (blue). **c)** HFFs co-expressing Flag-SFP1 and HA-GRA29 show SFP1 strands radiating from GRA29 foci. Immunofluorescence of co-transfected HFFs expressing Flag-SFP1 and HA-GRA29. Anti-SFP1 (green), anti-HA (magenta) and DAPI (blue).

233   These data indicate that both SFP1 and GRA29 can form filament-like structures in the absence

234   of other *Toxoplasma* proteins. Although we were unable to confirm the interaction in co-

235   immunoprecipitation or biochemical experiments (data not shown) the co-localisation of SFP1

236   and GRA29 even in this non-physiological context suggests that they can directly interact.

12

237   Furthermore, the localisation pattern observed in HFFs and the extended SFP1 filaments in

238   parasites lacking GRA29 suggest that GRA29 initiates SFP1 strand formation.

239   **The SFP1/GRA29 C terminal tail is required for strand formation**

240   The change of localisation of GRA29 upon C-terminal HA-tagging and the cluster of

241   phosphorylation sites in the C-termini of SFP1 and GRA29 suggested the C-terminal tail may

242   play an important role in the regulation of strand-formation. To address this, we expressed

243   truncated SFP1 and GRA29 lacking the unstructured C-terminal region in HFFs. In contrast to

244   forming filaments under these conditions, both proteins appeared distributed throughout the

245   HFF cytoplasm, with sparse foci of aggregation observed (Fig. 4A). This strongly suggested that

246   the C-terminus of the protein plays an important role in filament formation. Consistently,

247   during *Toxoplasma* infection with RHΔ*sfp1+*SFP1Δ*Ct* there was a lack of typical SFP1 strand

248   formation in the PV (Fig. 4B). However, SFP1Δ*Ct* appeared aggregated within the PV, rather

249   than dispersed, suggesting other PV resident proteins impact SFP1 distribution.

250   Having established that the C-terminus of SFP1 is important for its subcellular organisation, we

251   asked whether phosphorylation of SFP1 is important for filament formation. To investigate this,

252   we first turned to expression of phosphomutants in HFFs, in which all phosphorylation sites in

253   the SFP1 C-terminus were mutated to Alanine (SFP1_ALA) and phosphomimetics, in which all

254   phosphorylation sites were mutated to Glutamic acid (SFP1_GLU). While SFP-ALA mutants

255   displayed normal filaments in the HFFs, mimicking phosphorylation lead to an inability of SFP1

256   to form filaments. This indicates that phosphorylation may be a negative regulator of filament

257   formation (Fig. 4C). This was replicated when SFP1_ALA and SFP1_GLU were expressed in

13

258   RHΔ*sfp1* parasites (Fig. 4D), where extended strands were observed with phosphomutant but

259   not phosphomimetic mutations.

260
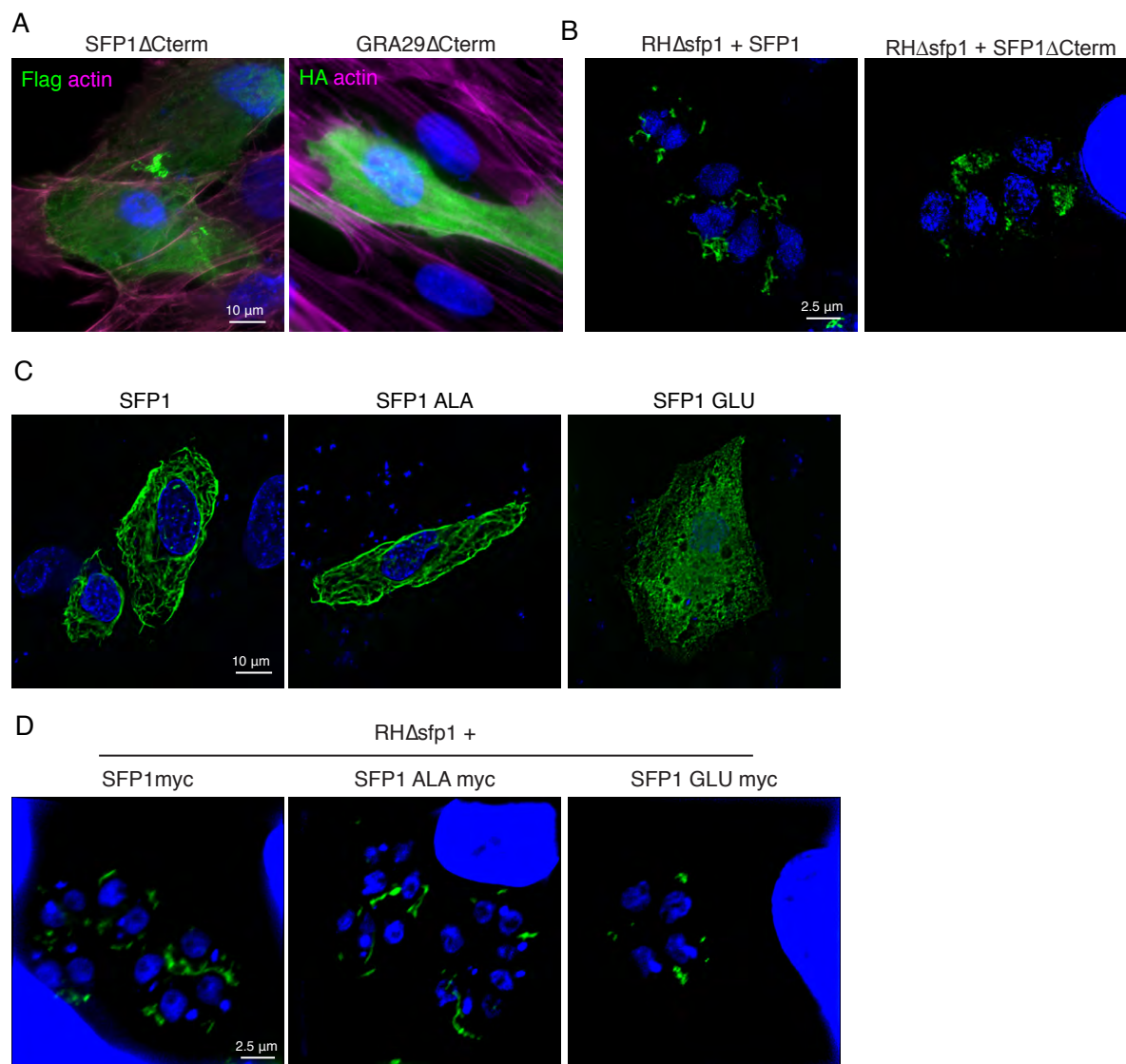
261   **Figure 4. SFP1 and GRA29 C-termini regulate strand formation. a)** Immunofluorescence
262   analysis of HFFs expressing truncated Flag-SFP1 or HA-GRA29 lacking their disordered C
263   termini. Anti-Flag or HA antibodies (green), Phalloidin (magenta) to visualise F-actin, and DAPI
264   (blue). **b)** SIM analysis of HFFs infected with RHΔ*sfp1* expressing SFP1-myc or SFP1ΔCterm-
265   myc. Anti-SFP1 antibodies (green) and DAPI (blue) **c)** SFP1 phosphomutants (preventing
266   phosphorylation) does not disrupt strand formation. Immunofluorescence analysis of HFFs
267   expressing Flag-SFP1, or Flag-SFP1 with the C-terminal phosphosites mutated to ALA or GLU.
268   Anti-Flag antibodies (green) and DAPI (blue). **d)** Immunofluorescence analysis of HFFs infected
269   with RHΔ*sfp1* expressing myc tagged SFP1, SFP1 ALA or SFP1 GLU. Anti-myc antibodies (green)
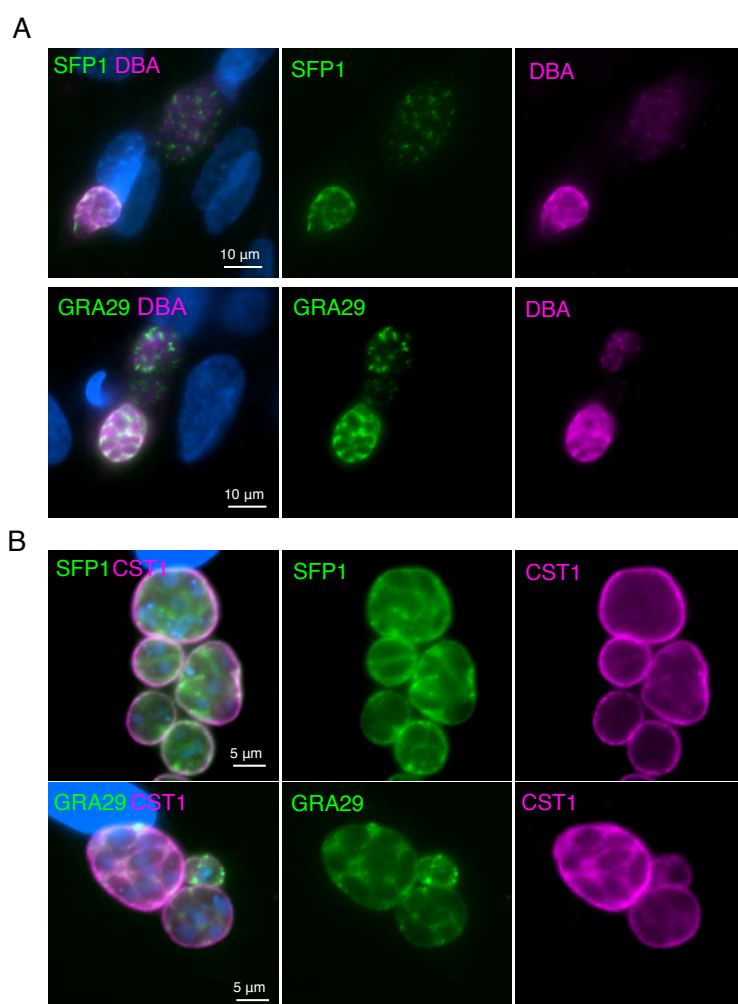270   and DAPI (blue).

14

271 If phosphorylation was preventing filament formation, we hypothesized that SFP1 and GRA29

272 expressed in HFFs should not be phosphorylated. To verify that assumption we

273 immunoprecipitated SFP1 from HFFs and analysed the proteins by mass-spectrometry. Despite

274 the presence of many non-modified peptides from SFP1, we observed no phosphopeptides

275 (data not shown), indicating that indeed, SFP1 is not phosphorylated by human kinases when

276 expressed in HFFs.

277 Collectively these data show that the C-termini of SFP1 and GRA29 are important for their

278 regulation and that phosphorylation appears as a negative regulator with the non-

279 phosphorylated protein forming strands.

280 **Secreted proteins are differentially phosphorylated in the chronic stage**

281 To determine whether SFP1 and GRA29 are required *in vivo*, we generated gene KOs in the

282 Type II strain Pru, and verified gene disruption by Western blot (Fig. S3A). Mice infected with

283 PruΔ*sfp1* and PruΔ*gra29* parasites succumbed to infection similarly to WT PruΔ*ku80* parasites

284 indicating neither protein is essential for parasite survival *in vivo* (Fig. S4B, C). During our

285 experiments with the Pru strains, we observed that in some vacuoles SPF1 and GRA29

286 appeared distributed throughout the PV space instead of forming characteristic strands (Fig.

287 5A). Type II strains differ from the type I RH strain in that they more frequently convert to slow-

288 growing bradyzoites in tissue culture. Bradyzoite cysts can be distinguished from tachyzoite

289 vacuoles using fluorescently labelled lectin (DBA) that binds to the cyst wall (25). Parasites with

290 a disperse SFP1/ GRA29 pattern also stained positive for the cyst-wall marker (Fig. 5A).

291 Spontaneous conversion to bradyzoites occurs at low levels in standard tissue culture but high

292 levels of conversion can be induced by pH stress (26). Under bradyzoite-inducing conditions

293 parasite vacuoles were positive for the cyst wall marker CST1, and showed disperse SFP1 and

15

294   GRA29 indicating that both proteins undergo a major change in localisation between the

295   tachyzoite and the bradyzoite stages (Fig.5B).

296

297   **Figure 5. SFP1 and GRA29 disperse in chronic stage cysts. a)** Immunofluorescence analysis of
298   HFFs infected with PruΔ*hxgrpt* for 40h. Anti- SFP1 or anti-GRA29 (green), DBA (red) to stain
299   the cyst wall and DAPI (blue). **b)** Immunofluorescence analysis of PruΔ*hxgrpt* infected HFFs
300   grown under bradyzoite inducing conditions for 3 days. Anti- SFP1 or anti-GRA29 (green) with
301   anti-CST1 (magenta) to visualise the cyst wall, and DAPI (blue).

302

303   We hypothesised that increased phosphorylation of SFP1 and GRA29 under bradyzoite

304   conditions could lead to their dispersion. This phenomenon of redistribution in the bradyzoite

305   cyst has been described for other GRAs and so we wanted to determine if these were also

306   differentially phosphorylated. We therefore used comparative phosphoproteomics to

16

307   determine differences in the phosphorylation of SFP1 and GRA29 and more broadly between

308   acute (tachyzoite) and chronic (bradyzoite) conditions. Triplicate samples of *Toxoplasma* were

309   grown in tachyzoite conditions for 27 h or bradyzoite conditions for 3 days (to give comparable

310   numbers of parasites per vacuole) (Fig. 6A). We performed quantitative mass spectrometry to

311   compare protein and phosphosite abundances between the two conditions using tandem mass

312   tags (TMT) as described in (27, 28). First, we analysed differential protein abundance and

313   identified 171 differentially regulated proteins with 103 proteins with higher abundance in

314   bradyzoites and 68 with higher abundance in tachyzoites. As expected, known bradyzoite

315   markers such as BAG1, ENO1, LDH2 and MAG1 were more abundant in the bradyzoite samples

316   compared to the tachyzoite samples (Table S1 and Fig. S5).

317

318   In the phosphopeptide enriched samples we quantified 7650 phosphorylation sites on 2235

319   *Toxoplasma* proteins. For 3730 of the phosphorylation sites we also obtained quantitative

320   proteome data to which phosphorylation site changes were normalized. This allowed us to

321   assess true differential phosphorylation rather than changes originating from differential

322   protein abundance between conditions. After this normalisation step, we identified 337

323   phosphorylation sites that were significantly different between tachyzoite (144 sites more

324   phosphorylated) and bradyzoite (193 sites more phosphorylated) stages (Fig. 6B, Table S1).

325   The 337 phosphorylation sites are found on 170 proteins, 51 of which are predicted to be

326   secreted (ROPs or GRAs in LOPIT dataset, ToxoDB). While GRAs made up 11% of proteins with

327   non-changing phosphosites, they represented 26% of differentially phosphorylated proteins

328   (Fig. 6C). This enrichment of GRAs in the subset of proteins that are differentially

329   phosphorylated between tachyzoite and bradyzoite conditions indicates that these are indeed

330   subject to extensive differential phosphorylation during stage conversion.

17

331
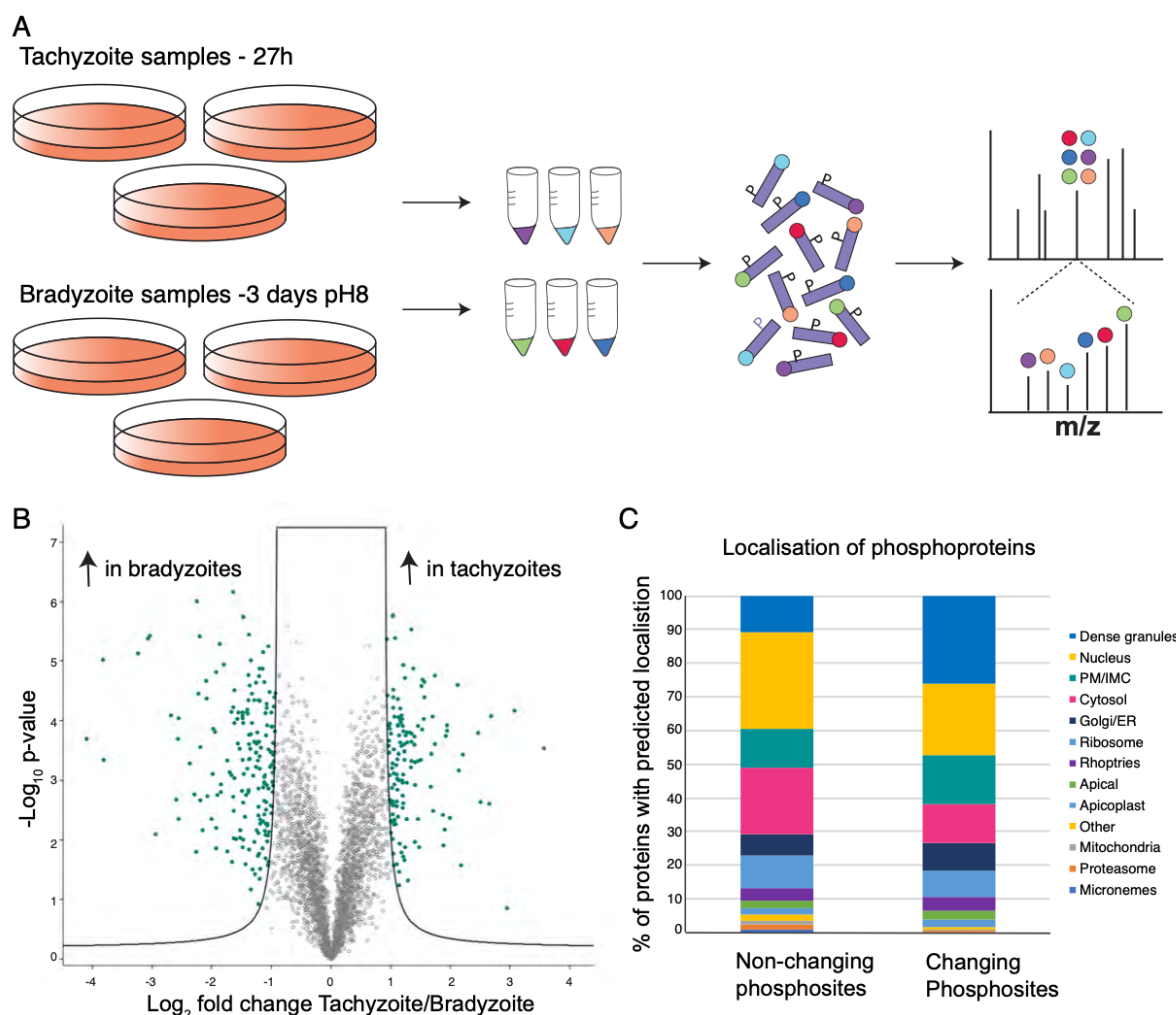
Figure 6. Secreted proteins are differentially phosphorylated in acute and chronic stages. a) Schematic of quantitative phosphoproteomics experiment. Peptides from triplicate tachyzoite and bradyzoites samples were labelled with tandem mass tags (TMT), enriched for phosphopeptides and analysed by mass spectrometry. **b)** Volcano plot showing differential phosphorylation between tachyzoite and bradyzoite conditions after normalisation to protein abundance. Each circle represents a phosphosite and those that change significantly (FDR 1%, -0.9> $\log_2$ fold change >0.9) are shown in green. **c)** Dense granule proteins are enriched in the subset of proteins that show significantly changing phosphorylation between tachyzoites and bradyzoites. Chart showing the predicted localisation of phosphoproteins using LOPIT (ToxoDB).

In this experiment we also identified phosphosites corresponding to the C-termini of SFP1 and GRA29, but they did not significantly change between conditions, (although a previously undetected N-terminal site on GRA29 was detected as more phosphorylated in bradyzoites).

18

346 However, the GRAs that were detected as differentially phosphorylated included the IVN

347 localised GRA2, GRA4, GRA6, GRA12, and PV membrane GRA1 and GRA5 (Table 1). We also

348 detected differential phosphorylation of the cyst wall proteins CST1, CST3, CST4 and CST6.

349 Furthermore, of the 38 recently identified putative cyst wall components (29), 24 were

350 differentially phosphorylated suggesting phosphorylation could play an important role in the

351 formation of this structure.

352

353 It is worth noting that we also observed differential phosphorylation on proteins important for

354 DNA regulation. This includes the AP2 domain transcription factors AP2VIII-2 and AP2XII-4, and

355 32 predicted nuclear proteins. These may be important for transcriptional regulation during

356 stage conversion, but their role is not further discussed here.

357

358 Collectively these data show that SFP1 and GRA29 undergo a dramatic change in localisation

359 between tachyzoite and bradyzoite conversion but that their phosphorylation is transient or

360 not required for this transition, at least at the experimental timepoint selected herein.

361 Furthermore, we show widespread changes in phosphorylation state in a substantial number

362 of secreted proteins, indicating the activity of stage-specific kinases and phosphatases in

363 regulating PV resident proteins.

364

365 **DISCUSSION**

366 Here we have analysed the localisation of two secreted phosphoproteins, SFP1 and GRA29 that

367 re-localise during stage conversion to bradyzoites. Both proteins form stranded structures in

368 the tachyzoite PV, that are distinct from the IVN and actin filaments previously observed. We

369 did not identify a function of SFP1 and GRA29 during the lytic cycle or *in vivo* infections,

19

370   preventing us from assessing the impact of their phosphorylation in *Toxoplasma* biology. It

371   could be that the proteins have a subtle effect on growth that we have not been able to

372   measure, or that they are important in another host-species, parasite stage or genetic

373   background we have not tested here. However, neither SFP1 nor GRA29 showed a reduction

374   in fitness *in vivo* (30) in our recent more sensitive *in vivo* CRISPR screen, supporting a non-

375   essential role under these conditions.

376   We show the importance of the C-termini of both proteins for strand formation. Using

377   mutational analysis, we show that SFP1 phosphorylation is not required for filament formation

378   and that mimicking phosphorylation disrupts filament formation. As such, mimicking

379   phosphorylation mirrored the phenotype observed with removal of the C-terminal tail. This

380   suggests that SFP1 and GRA29 form oligomers dependent on their un-phosphorylated C-

381   termini. Phosphorylation negatively regulates the intrinsic behaviour of SFP1 and GRA29 and

382   abrogates their ability to form multimers. However, as both proteins where identified to be

383   phosphorylated after secretion into the PV (19) where, as we show here, they form fibril-like

384   structures, we assume that their phosphorylation is a dynamic process, potentially leading to

385   the regulation of their length and location. It could also be that phosphorylated and non-

386   phosphorylated SFP1 and GRA29 localize to different structures in the PV. How both proteins

387   re-localise during stage conversion is unclear. While mimicking phosphorylation appears

388   sufficient to promote dispersal of SFP1 and GRA29 in HFFs, this is not observed when expressed

389   in tachyzoites, where an aggregation is observed. This indicates that other proteins, or post-

390   translational modifications are involved in SFP1/ GRA29 regulation in parasites upon stage

391   conversion.

392 Recently, the PV localised kinase WNG1/ROP35 was shown to phosphorylate several GRAs,

393 including GRA6, and to regulate their membrane association (20). As many GRAs form

394 complexes during trafficking (31), WNG1 phosphorylation is hypothesised to release them

395 from association with a chaperone, freeing them to associate with membranes. As such, WNG1

396 dependent phosphorylation of GRAs was shown to promote their normal behaviour and

397 localisation. We now propose that in addition to WNG1 phosphorylation promoting release

398 and membrane association of GRAs, phosphorylation of secreted proteins can negatively

399 regulate their behaviour. In this way, the parasite could use phosphorylation by kinases within

400 the PV lumen to regulate PV resident proteins. This would allow the parasite to tailor its niche

401 and respond to differing conditions or requirements.

402 Several secreted kinases localise within the PV lumen and are upregulated during the chronic

403 stages of infection (for example ROP21, ROP27, ROP28, and indeed WNG1/ROP35).

404 Importantly, secreted kinases have been shown to contribute to cyst formation in mice

405 indicating that phosphorylation within the PV/forming cyst is required for cyst development.

406 ROP21/27/28 contribute to the parasite establishing chronic infection but their function and

407 targets remain unknown (32). Additionally, a triple knockout of ROP38/29/19 showed a severe

408 defect in cyst formation (33). Here we expand our knowledge of cyst formation by reporting

409 the differential phosphorylation of proteins within the forming cyst. Our data also identifies

410 phosphorylation that is reduced upon stage conversion. The expression of many ROP family

411 kinases is reduced in the chronic stage of infection, which could account for some changes, but

412 it is likely that secreted phosphatases are contributing to the differential phosphorylation. The

413 necessity of deleting several ROPs to observe strong phenotypic effects in bradyzoites may

414 reflect that the system is flexible with a high degree of redundancy. Alternatively, the combined

415   effect of multiple kinases could allow the parasite to integrate several signals leading to stage

416   differentiation.

417   PV resident GRAs re-localise as the parasite converts to the chronic stage and remodels the PV

418   to form the cyst. Guevera *et al.,* recently described the dynamic nature of this re-localisation

419   over the course of cyst formation (for GRA1, 2, 4, 6, 9, 12) (21). Furthermore, they showed that

420   IVN localised GRAs were required for normal formation of the cyst wall. Here we show that

421   these GRAs, with the exception of GRA9 (which is upregulated in bradyzoites) are differentially

422   phosphorylated in the acute and chronic stages suggesting phosphorylation could play a role

423   in their regulation. Interestingly, GRA2 showed phosphorylation sites that were enriched in

424   each condition; two sites within a predicted amphipathic helix were more phosphorylated in

425   tachyzoite conditions, while a third site was more phosphorylated in the bradyzoite samples.

426   It is tempting to speculate that dual phosphorylation within the polar side of the amphipathic

427   helix (a1) of GRA2 could alter its membrane binding. Further work assessing phosphorylation

428   of secreted proteins over time is required to decipher the impact of this modification and the

429   role of both kinases and phosphatases in remodelling the PV. However, the regulation of

430   proteins after parasite secretion adds an intriguing extra layer of complexity to pathogen

431   effector biology and establishing *Toxoplasma* chronic infection.

432

MATERIALS AND METHODS

Cell culture and parasite strains

435   Primary human foreskin fibroblasts (HFFs) (ATCC) were maintained in Dulbecco's modified

436   Eagle's Medium (DMEM) with 4.5g/L glucose and GlutaMAX-1 (Gibco) supplemented with 10%

437   foetal bovine serum (FBS) at 37°C and 5% CO_2. T*. gondii* RHΔ*ku80*::diCre (34), RHΔ*gra2* (35),

438 PruΔ*ku80 (36)* and PruΔ*hxgprt* (gift from Dominique Soldati, as in (37)) parasites were

439 maintained by growth in confluent HFFs and passaged every 2-3 days. RH strains were seeded

440 24 h, and Pru strains 48 h, before transfections or infection experiments.

441

442 **Sequence analysis**

443 Gene sequences and predicted protein localisations (LOPIT dataset) were obtained from

444 ToxoDB. Alignments were generated using ClustalW and schematics using DOG2.0 (38). Protein

445 sequences were analysed by Multicoil2, (39)) and Globplot, (40) to identify coiled coil and

446 unstructured regions respectively. Protein schematics were generated

447

448 **Plasmid construction**

449 All primers are shown in Supplementary File 1. Vectors were generated by inverse PCR using

450 KOD Hot-start polymerase (Novagen) or by Gibson assembly in a homemade reaction master

451 mix (100 mM Tris-Cl pH 7.5, 50 mg/mL PEG-8000, 10 mM $MgCl_2$, 10 mM dithiothreitol, 0.2 mM

452 each of four dNTPs, 1 mM NAD with 0.8U T5 exonuclease (NEB), 0.5 U Phu DNA polymerase

453 (NEB) and 80 U Taq DNA ligase (NEB)). Gibson reactions were incubated for 60 min at 50°C. All

454 vectors were verified by sequencing. *sfp1* and *gra29* sequences were amplified from

455 *Toxoplasma* gDNA prepared from 1E7 RHΔ*ku80*::diCre parasites using Qiagen Blood and Tissue

456 DNA extraction kit, unless otherwise stated.

457

458 To generate pSFP1, the TGGT1_289540 promoter and coding sequence were amplified using

459 primers 1 &2 and inserted in to HindIII/PacI digested pGRA (12). A C terminal myc tag was

460 inserted by inverse PCR using primers 3 and 4. pSFP1ΔCterm was generated by inverse PCR on

461 pSFP1 with primers 4 & 5. To generate phosphomutant versions of pSFP1, initially a silent ApaI

23

462   site was inserted into pSFP1 (at nt2529) by inverse PCR with primers 6 & 7. 400bp synthetic

463   DNA fragments (IDT, Supplementary file 1) encoding SFP1-myc C-terminal or versions with

464   Ser/Thr to ALA, or Ser/Thr to GLU mutations were mixed with ApaI/PacI digested pSFP1 ApaI

465   in Gibson reaction mix. pGRA29-HA was generated by amplifying GRA29 promoter and coding

466   sequence using primers 8 & 9 and inserting the amplicon in to HindIII/NcoI digested pGRA.

467

468   For pcDNA-NTAP-Flag SFP1 constructs, the SFP1 coding sequence excluding the signal peptide

469   was amplified with primers 10 & 11 for full length or primers 10 & 12 for C terminal truncated

470   versions. For phosphosite mutant versions primers 10 & 11 were used with pSFP1 ALA or pSFP1

471   GLU as the template. All amplicons were inserted into NotI/EcoRI digested pcDNA-NTAP, a

472   pcDNA3.1 derivative for expression with 3x Flag tag, TEV cleavage site and calmodulin binding

473   peptide. For pcDNA-HA-GRA29 construct, GRA29 was initially amplified with primers 13 & 14

474   and inserted into NotI/EcoRI digested pcDNA-NTAP. The Flag tag was removed and an N-

475   terminal HA tag inserted by inverse PCR with primers 15 & 16. pcDNA-GRA29ΔCterm was

476   generated by inverse PCR with primers 17 & 18.

477

478   gRNA sequences targeting the 5' and 3' of *sfp1*/*gra29* were inserted into pSAG1::CAS9-

479   U6::gUPRT (41) by inverse PCR with primers 19 & 20-23. Dual gRNA pSAG1::CAS9 vectors were

480   generated by amplifying 3' gRNA expression locus with primers 24 & 25 and inserting the

481   region into XhoI/PacI digested pSAG1::CAS9 carrying the 5' gRNA.

482

483   To generate the SFP1 bacterial expression plasmid, pET-28a-SFP1, SFP1 lacking its amino

484   terminal signal peptide was amplified using primers 26 & 27. The amplicon was cloned

485   into *BamHI* and *NdeI* digested pET-28a(+) plasmid (Merck).

24

486

Parasite transfection

488 Parasites were released from HFFs by syringe lysis, pelleted at 650 x g and resuspended in

489 cytomix (10mM KPO4, 120mM KCl, 0.15mM CaCl2, 5mM MgCl2, 25mM Hepes, 2mM EDTA).

490 ~5E6 parasites were combined with 40 ug DNA in 400ul cytomix in a 2mm cuvette and

491 electroporated using a Bio-Rad Gene Pulser Xcell at 1500 V, and 25 uF. Repair templates were

492 linearised by overnight digestion, purified by phenol-chloroform precipitation and

493 resuspended in H_2O. 24h post transfection 50 μg/ml Mycophenolic acid (Merck) and Xanthine

494 (Sigma) (M/X) were added to select for transfectants.

495

Generating parasite lines

497 RHΔku80 lacking SFP1 was generated by transfecting parasites with pSAG1-CAS9sgSFP1

498 targeting the 5' end of the gene (starting 84nt after ATG) with a 183nt repair template to

499 remove the PAM site and introduce STOP codons (seq in supp file?). Parasites expressing the

500 transfected Cas9-GFP were sorted by flow cytometry into 96 well plates containing HFF

501 monolayers using a BD Influx cell sorter (BD Biosciences). This line was used for complementing

502 pSFP1myc constructs. Alternatively, gra29 and sfp1 were disrupted in RHΔku80 and PruΔku80

503 backgrounds by co-transfecting a double gRNA pCAS9 vector targeting the 5' and 3' of the gene

504 and a synthetic repair construct with 500 nt homology arms and HXGPRT- T2A-mCherry

505 cassette (GeneArt, Life Technologies). Transfectants were selected by the addition of M/X, and

506 clones were screened by immunofluorescence and verified by western blot.

507

Antibody generation

509   N-terminal 6xHis tagged SFP1 recombinant protein was expressed form pET-28a-SFP1

510   in *Escherichia coli* BL21 cells. His-SFP1 was purified using Ni-NTA affinity purification under

511   native conditions using the standard manufacturer's protocol (Qiagen). Recombinant His-SFP1

512   was used to immunize female New Zealand white rabbits (Covalab) for generation of polyclonal

513   antibodies. To generate the mouse anti-SFP1 antibody, phosphopeptides corresponding to the

514   C-terminal of SFP1 were conjugated to Keyhole limpet hemocyanin and used to immunise 4

515   mice (Covalab). Day 53 sera showed reactivity against SFP1. While mice were immunized with

516   phosphorylated isoforms, the antibodies recognise non-phosphorylated peptides.

517   SFP1 peptides used for immunisation. Residues in bold were phosphorylated.

518   *NH2-C-GSVA**S**GFRG -CONH2*

519   *NH2-C-GFRG**S**MA**S**GLFP - CONH2*

520   *NH2-C-LRGA**S**VAG**S**LGG -CONH2*

521   *NH2-C-GGVG**S**RLGG-CONH2*

522   *NH2- C-FAGA**S**MGRG*-CONH2

523

524   **Immunoprecipitation**

525   HFFs were infected with RHΔ*ku80* or RHΔ*ku80* +SFP1::myc in a T25 flask for 24h before lysis in

526   1ml RIPA buffer (Thermoscientific) supplemented with protease (complete mini, Roche)

527   inhibitors. Samples were clarified by centrifugation and incubated with anti-Myc tag antibody

528   conjugated agarose (Millipore, Cat. no. 16-219) for 3h. The non-bound fraction was removed

529   and the proteins precipitated with acetone at -20 °C. Agarose bead complexes were washed in

530   RIPA buffer followed by Tris buffer saline and proteins eluted by boiling in Laemmli buffer (60

531   mM Tris-HCl pH6.8, 1% SDS, 5% glycerol, 5% b-mercaptoethanol, 0.01% bromophenol blue).

532

Western blotting

534 *Toxoplasma* lysates or IP samples were separated by SDS-PAGE, transferred onto nitrocellulose

535 (BioRad) and probed with appropriate antibodies in PBS with 3% milk and 0.1% Tween20

536 (Sigma-Aldrich). Rabbit and mouse anti-SFP1 serum were used at a dilution of 1:1000, rabbit

537 anti-GRA29 serum at 1:1000 (ref CRISPR paper?), mouse anti-GRA1 at 1: 1000 (gift from Jean-

538 Francois Dubremetz), mouse anti-GRA2 at 1:1000 (Biotem BIO.018.5), mouse anti-Myc at

539 1:1000 (Millipore, 05-724), and rat anti-HA at 1:1000 (Roche, 11867423001). After washing,

540 the blots were incubated with HRP-conjugated secondary antibodies; anti-rabbit at 1:20,000

541 (Insight Biotechnology, Cat no. 474-1506), anti-mouse at 1:3,000 (Insight Biotechnology, Cat

542 no. 474-1506) or anti-rat at 1:4000 (Life technologies, Cat. no 629520). The blots were

543 visualised using ECL Western Blotting Detection Reagent (GE Healthcare) for

544 chemiluminescence imaging on an Amersham Imager 600 (GE-Healthcare).

545

Parasite infections

547 For widefield, confocal or EM imaging HFFs were seeded on 13mm #1.5 coverslips in 24 well

548 plates. Confluent monolayers were infected at a multiplicity of infection (MOI) of 1 for 16-24

549 h. For Cytochalisin D treatment infected cells were incubated with 1 μM Cytochalasin D or

550 DMSO for 1h before fixation. Samples were washed with PBS before fixation in 3%

551 formaldehyde (FA) for 15 min. For EM analysis, infected cells were fixed in 4% FA for 15min

552 followed by 2.5% glutaraldehyde/4% FA for 30min and storage in 1% FA.

553

Conversion to bradyzoites

555 To induce parasite switching to bradyzoites, HFF monolayers were infected at an MOI of 0.5

556 for 3.5h then washed four times with PBS before adding switch media (RPMI (Sigma, R4130)

557   with 1% FBS, pH 8.1) and incubating at 37°C and ambient CO_2 for 3 days. Cells were fixed in 3%

558   FA, quenched in 50mM ammonium chloride and permeabilised in 0.2% triton, 0.1% glycine

559   0.2% BSA in PBS for 20 mins on ice.

560

561   **Intracellular fluorescent protein ingestion assay**

562   Intracellular fluorescent protein ingestion was assessed as described in McGovern et al. (42).

563   Briefly, 70-80% confluent CHO-K1 cells were transfected in 35 mm dishes using X-TREMEGENE

564   9 Transfection Reagent (Roche, 6365787001). Each dish was transfected with 2 µg of pCDNA

565   3.1 Venus plasmid using the using a 3:1 ratio of plasmid to transfection reagent in Opti-MEM

566   (Gibco, 31985062) and a total final volume of 200 µl. The CHO K1 cells were then incubated

567   overnight at 37°C and synchronously infected with *T. gondii* parasites using the ENDO Buffer

568   Method at 18 to 24h post-transfection (43). *T. gondii* parasites were treated with 1 µM LHVS or

569   equal volume of DMSO for 48h prior to synchronous invasion, replacing the LHVS and DMSO-

570   treated media every 6-18h, and also during the 3h incubation period after synchronous

571   invasion. *T. gondii* parasites were purified at 3h post-invasion as previously described (16),

572   pelleted by centrifugation at 1000xg for 10 min at 4°C, and subjected to a protease protection

573   assay by resuspension in 250 µl of freshly prepared 1 mg/mL Pronase (Roche,

574   10165921001)/0.01% Saponin/PBS at 12°C for 1h. The parasites were then pelleted by

575   centrifugation at 1000*xg* for 10 min and washed 3 times in ice cold PBS before depositing on

576   Cell-Tak (Corning, 354240) coated chamber slides. Parasites were fixed with 4%

577   paraformaldehyde imaged with an AxioCAM MRm camera-equipped Zeiss Axiovert Observer

578   Z1 inverted fluorescence microscope. Ingestion of host cytosolic Venus was scored manually

579   as Venus-positive or Venus-negative without sample blinding.

580

28

581   **HFF transfection**

582   HFFs were seeded at a density of 7.5 x10^4 cells per well on a 13mm glass coverslip 24h before

583   transfection with Lipofectamine 2000 (Thermofisher). For each well 1.5 μl Lipofectamine 200

584   was mixed with 800 ng plasmid DNA in 100 μl Optimem (Thermofisher). Cells were fixed in 3%

585   FA 18h post transfection.

586

587   **Immunofluorescence analysis**

588   For immunofluorescence analysis cells were quenched in 50mM ammonium chloride for

589   15min. Transfection experiments and initial RHΔ*ku80* +SFP1::myc or RHΔ*ku80* +GRA29::HA

590   infections were permeabilised for 3min in 0.1% triton and blocked with 2% BSA in PBS. For

591   subsequent infection experiments samples were permeabilised and probed in 0.05 % saponin,

592   0.2% fish gelatin in PBS. Infected or transfected cells were probed with mouse anti-Myc

593   (1:1000, Millipore 05-724), rat anti-HA (1:1000, Roche, 11867423001), mouse anti-Flag

594   (1:1000, Sigma F1804), rabbit anti-GRA29 (1:4000,(30)), rabbit anti-SFP1 serum (1:1000),

595   mouse anti-SFP1 (1:200), or mouse anti-CST1 (1:100, gift from Louis Weiss) followed by

596   Alexafluor488 or 564 conjugated secondary antibodies (1:2000, Life Technologies).

597   Additionally, cells were labelled with DAPI (1:1000 of 5mg/ml, Sigma Aldrich), Alexa647

598   conjugated Phalloidin (1:100, Invitrogen A22287) or Rhodamine conjugated Dolichos Biflorus

599   Agglutinin (1:200, Vector Labs RL-1302). Antibodies/stains were diluted in 2% BSA PBS and

600   samples were incubated for 1h and coverslips were subsequently washed and mounted with

601   ProLong Gold anti-Fade moutant (Thermofisher, P36934). Localisations were visualised on a Ti-

602   E Nikon microscope or Leica SP5 Confocal.

603

604   **Super resolution microscopy**

605 For super resolution microscopy 24 x 24 #1.5H coverslips were washed in 1M HCl overnight,

606 rinsed in water before coating with 1% (w/v) porcine gelatin (Sigma, G1890) in 6 well plates.

607 Confluent HFF monolayers were infected with an MOI of 0.5 and centrifuged at 180 x g for 3

608 min to synchronise infection. Samples were fixed and processed as above except that antibody

609 dilutions were passed through 0.45 μM filters and an additional final fixation step (10 min, 2 %

610 FA) was included after secondary antibody incubation. Super-resolution microscopy imaging

611 was performed using an OMX v3 structured illumination microscope (Applied Precision/GE

612 Healthcare) equipped with 405, 488 and 592.5 nm diode lasers, electron multiplying CCD

613 cameras (Cascade II 512 × 512, Photometrics) and a 100×/1.40 NA PlanApochromat oil-

614 immersion objective lens (Olympus). 3D-SIM image stacks were reconstructed and aligned

615 using softWoRx (Applied Precision/GE Healthcare).

616

617 **Correlative Light and Electron Microscopy**

618 HFFs were seeded on a 3.5 cm dish with gridded coverslip (MatTek) and infected, fixed and

619 processed as described above. Regions of interest with GRA29-HA cage structures were

620 selected and imaged by SIM. Tiled images of the surrounding area were generated by Confocal

621 imaging to aid in identifying the region by EM. The cells were then fixed and prepared for EM

622 as described below. The light and electron microscopy overlay was generated using the

623 TurboReg plugin of Fiji software, with an affine transformation using the parasite nuclei and

624 apicoplasts as landmarks, and by selecting high intensity pixels in Photoshop using the magic

625 wand tool with tolerance set to 40.

626

627 **EM sample preparation and imaging**

628   Cells were fixed in 2.5% glutaraldehyde, 4% formaldehyde in 0.1 M phosphate buffer (PB) at

629   room temperature for 30 min, post-fixed in 1% reduced osmium tetroxide for 1 h, stained with

630   1% tannic acid in 0.05 M PB for 45 min, and quenched with 1% sodium sulphate in 0.05 M PB

631   for 5 min. For CLEM experiments, the gridded coverslip was then removed from the MatTek

632   dish. After washing in PB and water, the cells were dehydrated in 70, 90, and 100% ethanol

633   (2x5 min each) before infiltration with a 1:1 mix of propylene oxide and Epon resin (Taab

634   Embed 812) for 1 h and then 2x90 min with Epon resin. Finally, coverslips were embedded in

635   resin for 24 h at 60ºC, sectioned (70–75 nm), and stained with lead citrate. Images were

636   acquired using a Tecnai Spirit Biotwin (Thermofisher Scientific) transmission electron

637   microscope.

638

639   *In vivo* infections

640   C57BL/6 (wild type) mice were bred and housed under pathogen-free conditions in the

641   biological research facility at the Francis Crick Institute in accordance with the Home Office UK

642   Animals (Scientific Procedures) Act 1986. All work was approved by the UK Home Office

643   (project license PDE274B7D), the Francis Crick Institute Ethical Review Panel, and conforms to

644   European Union directive 2010/63/EU. All mice used in this study were male and between 7-

645   to 9-week-old.

646   Mice were infected with PruΔ*ku80*, PruΔ*sfp1* or PruΔ*gra29* tachyzoites by intraperitoneal

647   injection (i.p.) with either 3E5 or 5E4 parasites in 200 µl PBS on day 0 to assess mouse survival.

648   Mice were monitored and weighed regularly for the duration of the experiments.

649

650   **Mass spectrometry**

651   **SFP1 transfection and Immunoprecipitation**

652   2.8×10^6 HFFs were seeded in a 15 cm dish 24 h before transfection with 44 ug pcDNA-SFP1

653   using Lipofectamine 3000 (Thermofisher) as per manufacturer's instructions. 18h post

654   transfection, cells were lysed on ice with 2 ml Immunoprecipitation (IP) buffer

655   (Thermoscientific) for 30min, passed through a 23 G needle and clarified by centrifugation. The

656   supernatant was incubated with 60ul of polyclonal SFP1 antibody coated Fast flow protein G

657   sepharose (GE Healthcare). Sepharose bead complexes were washed in IP buffer followed by

658   Tris buffer saline and proteins eluted by boiling in Laemmli buffer.

659   **In-gel digestion and LC-MS/MS**

660   Eluted proteins were separated by sodium dodecyl sulfate polyacrylamide gel electrophoresis

661   (SDS-PAGE), until the running front had migrated approximately 2 cm into the gel (12%

662   NuPAGE, Invitrogen), and stained with colloidal Coomassie (InstantBlue, Expedeon). After

663   excision of 8 horizontal gel slices per lane, proteins were in-gel digested with trypsin

664   (Promega/Pierce) using a Janus liquid handling system (Perkin Elmer). Tryptic peptides were

665   analyzed by liquid chromatography-mass spectrometry (LC–MS) using an Orbitrap Velos mass

666   spectrometer coupled to an Ultimate 3000 uHPLC equipped with an EASY-Spray nanosource

667   (Thermo Fisher Scientific) and acquired in data-dependent mode.

668

669   **MS Data Processing and Analysis**

670   The data were searched against *Toxoplasma gondii* and *Homo sapiens* (both Uniprot)

671   databases using the Andromeda search engine. Raw data were processed with MaxQuant

672   (version 1.5.2.8). Cysteine carbamidomethylation was selected as a fixed modification.

673   Methionine oxidation, acetylation of protein N-terminus and phosphorylation (S, T, Y) were

674   selected as variable modifications. The enzyme specificity was set to trypsin with a maximum

675   of 2 missed cleavages. The datasets were filtered on posterior error probability to achieve a

676   1% false discovery rate on protein, peptide and site level. Data were further analysed with

677   Perseus (version 1.5.0.9). The data were filtered to remove common contaminants and IDs

678   originating from reverse decoy sequences and only identified by site. The log10 values for

679   peptide intensities were then determined and all SFP1 peptides (58% sequence coverage)

680   analysed based on their modification state. No phosphorylated peptides were found.

681

682   **Tachyzoite v bradyzoite phosphoproteome**

683   **Infection conditions**

684   Confluent HFF monolayers were grown in 15 cm dishes and infected with PruΔ*hxgprt*. For

685   tachyzoite samples three dishes were infected with 1.3x10^7 parasites and incubated for 27h.

686   For bradyzoite samples three plates were infected 1.1 x10^7 parasites for 3.5 h before extensive

687   washing and the addition of switch media (described above). Bradyzoite infections were

688   incubated as above for 3 days with fresh switch media added daily.

689

690   **Cell lysis and protein digestion**

691   Lysis was performed in ice cold 8 M urea, 75 mM NaCl, 50 mM Tris, pH 8.2, supplemented with

692   protease (complete mini, Roche) and phosphatase (Phos Stop, Roche) inhibitors. Lysis was

693   followed by sonication to reduce sample viscosity (30% duty cycle, 3 x 30 seconds bursts, on

694   ice). Protein concentration was measured using a BCA protein assay kit (Pierce). Lysates (1mg

695   each) were subsequently reduced with 5 mM DTT for 30 min at 56 ^{o}C and alkylated in the dark

696   with 14 mM iodoacetamide for 30 min at RT. Following iodoacetamide quenching with 5 mM

697   DTT for 15 min in the dark, lysates were diluted with 50 mM ammonium bicarbonate to < 4M

698   urea, and digested with LysC (Promega) for 2-3h at 37 ^{o}C. Lysates were further diluted with 50

699   mM ammonium bicarbonate to <2M urea and digested with trypsin (Promega) overnight at

700   37°C. After digestion, samples were acidified with trifluoroacetic acid (TFA) (Thermo Fisher

701   Scientific) to a final concentration of 1% (v/v). All insoluble material was removed by

702   centrifugation and the supernatant was desalted on Sep-Pak C18 cartridges (Waters).

703

704   **TMT labelling**

705   Samples were dissolved at 1 mg/ml in 50 mM Na-HEPES, pH 8.5 and 30% acetonitrile (v/v) and

706   labelled with respective TMT reagents (Thermo Fisher Scientific, 2.4 mg reagent/1 mg sample)

707   for 1h at RT. Labelling was then quenched with 0.3% hydroxylamine for 15 min at RT and

708   samples acidified (pH~2) with formic acid. After verification of labelling efficiency via mass

709   spectrometry, the lysates were mixed in a 1:1 ratio, vacuum dried and desalted on Sep-Pak C18

710   cartridges.

711

712   **Phosphopeptide enrichment**

713   Desalted and vacuum dried samples were solubilized in 1 ml of loading buffer (80% acetonitrile,

714   5% TFA, 1 M glycolic acid) and mixed with 5 mg of TiO_2 beads (Titansphere, 5 μm GL Sciences

715   Japan). Samples were incubated for 10 min with agitation, followed by a 1 min 2000 × g spin

716   to pellet the beads. The supernatant was removed and used for a second round of enrichment

717   as explained below. Beads were washed with 150 μl loading buffer followed by two additional

718   washes, the first with 150 μl 80% acetonitrile, 1% TFA and the second with 150 μl 10%

719   acetonitrile, 0.2% TFA. After each wash, beads were pelleted by centrifugation (1 min at 2000

720   × g) and the supernatant discarded. Beads were dried in a vacuum centrifuge for 30 minutes

721   followed by two elution steps at high pH. For the first elution step, beads were mixed with 100

722   μl of 1% ammonium hydroxide (v/v) and for the second elution step with 100 μl of 5%

723   ammonium hydroxide (v/v). Each time beads were incubated for 10 min with agitation, and

724   pelleted at 2000 × g for 1 min. The two elutions were removed following each spin, and

725   subsequently pooled together before undergoing vacuum drying. The supernatant from the

726   TiO$_2$ enrichment was desalted on Sep-Pak C18 and the High Select Fe-NTA phosphopeptide

727   enrichment kit (Thermo Fisher Scientific) was used according to manufacturer's instructions

728   for a second round of enrichment.

729

730   **Sample fractionation and desalting**

731   Combined TiO$_2$ and Fe-NTA phosphopeptide eluates (phosphoproteome) as well as 100 μg of

732   the post-enrichment supernatant (total proteome) were fractionated using the Pierce High pH

733   Reversed-Phase kit (Thermo Fisher Scientific) according to manufacturer's instructions.

734   Resulting fractions, 8 for each phospho- and total proteome, were taken to dryness by vacuum

735   centrifugation and further desalted on a stage tip using Empore C18 discs (3M). Briefly, each

736   stage tip was packed with one C18 disc, conditioned with 100 μl of 100% methanol, followed

737   by 200 μl of 1% TFA. The sample was loaded in 100 μl of 1% TFA, washed 3 times with 200 μl

738   of 1% TFA and eluted with 50 μl of 50% acetonitrile, 5% TFA. The desalted phosphoproteome

739   and total proteome fractions were vacuum dried in preparation for LC-MS/MS analysis.

740

741   **LC-MS/MS and data processing**

742   Samples were resuspended in 0.1% TFA and loaded on a 50 cm Easy Spray PepMap column (75

743   μm inner diameter, 2 μm particle size, Thermo Fisher Scientific) equipped with an integrated

744   electrospray emitter. Reverse phase chromatography was performed using the RSLC nano

745   U3000 (Thermo Fisher Scientific) with a binary buffer system (solvent A: 0.1% formic acid, 5%

746   DMSO; solvent B: 80% acetonitrile, 0.1% formic acid, 5% DMSO) at a flow rate of 250 nl/minute.

747   The samples were run on a linear gradient of 5-60% B in 150 min with a total run time of 180

748   min including column conditioning. The nanoLC was coupled to an Orbitrap Fusion Lumos mass

749   spectrometer using an EasySpray nano source (Thermo Fisher Scientific). The Orbitrap Fusion

750   Lumos was operated in data-dependent mode using 3 acquisition methods. Phospho MS2

751   method: HCD MS/MS scans (R=50,000) were acquired after an MS1 survey scan (R=120, 000)

752   using MS1 target of 4E5 ions, and MS2 target of 2E5 ions. The number of precursor ions

753   selected for fragmentation was determined by the "Top Speed" acquisition algorithm with a

754   cycle time of 3 seconds, and a dynamic exclusion of 60 seconds. The maximum ion injection

755   time utilized for MS2 scans was 86 ms and the HCD collision energy was set at 38. Phospho

756   MS3 method: CID MS/MS scans (R=30,000) were acquired after an MS1 survey scan with

757   parameters as above. The MS2 ion target was set at 5E4 with multistage activation of the

758   neutral loss (H3PO4) enabled. The maximum ion injection time utilized for MS2 scans was 80

759   ms and the CID collision energy was set at 35. HCD MS3 scan (R=60,000) was performed with

760   synchronous precursor selection enabled to include up to 5 MS2 fragment ions. The ion target

761   was 1E5, maximum ion injection time was 105 ms and the HCD collision energy was set at 65.

762   Proteome MS2 method: same as Phospho MS2 with the following modification to MS2 target

763   5E4 ions. Acquired raw data files were processed with MaxQuant (44) (version 1.5.2.8) and

764   peptides were identified from the MS/MS spectra searched against *Toxoplasma gondii*

765   (ToxoDB) and *Homo sapiens* (UniProt) proteomes using Andromeda (45) search engine. TMT

766   based experiments in MaxQuant were performed using the 'reporter ion MS2 or MS3' built-in

767   quantification algorithm with reporter mass tolerance set to 0.003 Da. Cysteine

768   carbamidomethylation was selected as a fixed modification. Methionine oxidation, acetylation

769   of protein N-terminus, deamidation (NQ) and phosphorylation (S, T, Y) were selected as

770   variable modifications. The enzyme specificity was set to trypsin with a maximum of 2 missed

771   cleavages. The precursor mass tolerance was set to 20 ppm for the first search (used for mass

772   re-calibration) and to 4.5 ppm for the main search. 'Match between runs' option was enabled

773   for fractionated samples (time window 0.7 min). The datasets were filtered on posterior error

774   probability to achieve a 1% false discovery rate on protein, peptide and site level. Data were

775   further analyzed as described in the Results section and in the Supplementary Table S1 using

776   Microsoft Office Excel 2016 and Perseus (46) (version 1.5.0.9).

777

Data availability

779   The data behind this manuscript is freely available. The processed proteome and

780   phosphoproteome data is included in Table S1 and we are in the process of placing the raw

781   data on the PRIDE database.

782

Declaration of interest

784   The authors declare no competing interests.

785

Acknowledgements

798

799   **Figure legends: contained in the main text**

800   **Supplemental figure legends: in Supplementary figures file**

801   **Supplemental Material**

802   Supplementary figures – Fig S1 to S5

803   Table S1. TvB proteome_phosphoproteome

804   Supplementary File 1 – Oligonucleotides and synthetic DNA sequences used in this study.

805

806

807

REFERENCES

1. Pappas G, Roussos N, Falagas ME. 2009. Toxoplasmosis snapshots: Global status of Toxoplasma gondii seroprevalence and implications for pregnancy and congenital toxoplasmosis. International Journal for Parasitology 39:1385–1394.

2. Montoya J, Liesenfeld O. 2004. Toxoplasmosis. The Lancet 363:1965–1976.

3. Holland GN. 1999. Reconsidering the pathogenesis of ocular toxoplasmosis. American Journal of Ophthalmology 128:502–505.

4. Grigg ME, Ganatra J, Boothroyd JC, Margolis TP. 2001. Unusual Abundance of Atypical Strains Associated with Human Ocular Toxoplasmosis. J Infect Dis 184:633–639.

5. Dubey JP, Beattie CP. 1988. Toxoplasmosis of animals and man. Toxoplasmosis of animals and man.

6. Hakimi M-A, Olias P, Sibley LD. 2017. Toxoplasma Effectors Targeting Host Signaling and Transcription. Clinical Microbiology Reviews 30:615–645.

7. Mercier C, Cesbron-Delauw M-F. 2015. Toxoplasma secretory granules: one population or more? Trends in Parasitology 31:60–71.

8. Peixoto L, Chen F, Harb OS, Davis PH, Beiting DP, Brownback CS, Ouloguem D, Roos DS. 2010. Integrative Genomic Approaches Highlight a Family of Parasite-Specific Kinases that Regulate Host Responses. Cell Host & Microbe 8:208–218.

9. Gold DA, Kaplan AD, Lis A, Bett GCL, Rosowski EE, Cirelli KM, Bougdour A, Sidik SM, Beck JR, Lourido S, Egea PF, Bradley PJ, Hakimi M-A, Rasmusson RL, Saeij JPJ. 2015. The Toxoplasma Dense Granule Proteins GRA17 and GRA23 Mediate the

Movement of Small Molecules between the Host and the Parasitophorous Vacuole. Cell Host & Microbe 17:642–652.

10. Franco M, Panas MW, Marino ND, Lee M-CW, Buchholz KR, Kelly FD, Bednarski JJ, Sleckman BP, Pourmand N, Boothroyd JC. 2016. A Novel Secreted Protein, MYR1, Is Central to Toxoplasma's Manipulation of Host Cells. mBio 7:e02231-15.

11. Marino ND, Panas MW, Franco M, Theisen TC, Naor A, Rastogi S, Buchholz KR, Lorenzi HA, Boothroyd JC. 2018. Identification of a novel protein complex essential for effector translocation across the parasitophorous vacuole membrane of Toxoplasma gondii. PLOS Pathogens 14:e1006828.

12. Coppens I, Dunn JD, Romano JD, Pypaert M, Zhang H, Boothroyd JC, Joiner KA. 2006. Toxoplasma gondii Sequesters Lysosomes from Mammalian Hosts in the Vacuolar Space. Cell 125:261–274.

13. Sibley LD, Niesman IR, Parmley SF, Cesbron-Delauw MF. 1995. Regulated secretion of multi-lamellar vesicles leads to formation of a tubulo-vesicular network in host-cell vacuoles occupied by Toxoplasma gondii. Journal of Cell Science 108:1669–1677.

14. Mercier C, Dubremetz J-F, Rauscher B, Lecordier L, Sibley LD, Cesbron-Delauw M-F. 2002. Biogenesis of Nanotubular Network in ToxoplasmaParasitophorous Vacuole Induced by Parasite Proteins. MBoC 13:2397–2409.

15. Mercier C, Howe DK, Mordue D, Lingnau M, Sibley LD. 1998. Targeted Disruption of the GRA2 Locus inToxoplasma gondii Decreases Acute Virulence in Mice. Infection and Immunity 66:4176–4182.

16. Dou Z, McGovern OL, Cristina MD, Carruthers VB. 2014. Toxoplasma gondii Ingests and Digests Host Cytosolic Proteins. mBio 5.

17. Nolan SJ, Romano JD, Coppens I. 2017. Host lipid droplets: An important source of lipids salvaged by the intracellular parasite Toxoplasma gondii. PLOS Pathogens 13:e1006362.

18. Romano JD, Nolan SJ, Porter C, Ehrenman K, Hartman EJ, Hsia R, Coppens I. 2017. The parasite Toxoplasma sequesters diverse Rab host vesicles within an intravacuolar network. J Cell Biol 216:4235–4254.

19. Treeck M, Sanders JL, Elias JE, Boothroyd JC. 2011. The Phosphoproteomes of Plasmodium falciparum and Toxoplasma gondii Reveal Unusual Adaptations Within and Beyond the Parasites' Boundaries. Cell Host & Microbe 10:410–419.

20. Beraki T, Hu X, Broncel M, Young JC, O'Shaughnessy WJ, Borek D, Treeck M, Reese ML. 2019. Divergent kinase regulates membrane ultrastructure of the Toxoplasma parasitophorous vacuole. PNAS 116:6361–6370.

21. Guevara RB, Fox BA, Falla A, Bzik DJ. 2019. Toxoplasma gondii Intravacuolar-Network-Associated Dense Granule Proteins Regulate Maturation of the Cyst Matrix and Cyst Wall. mSphere 4.

22. Franco M, Shastri AJ, Boothroyd JC. 2014. Infection by Toxoplasma gondii Specifically Induces Host c-Myc and the Genes This Pivotal Transcription Factor Regulates. Eukaryotic Cell 13:483–493.

23. Periz J, Whitelaw J, Harding C, Gras S, Del Rosario Minina MI, Latorre-Barragan F, Lemgruber L, Reimer MA, Insall R, Heaslip A, Meissner M. 2017. Toxoplasma gondii

F-actin forms an extensive filamentous network required for material exchange and parasite maturation. eLife 6:e24119.

24. Nadipuram SM, Kim EW, Vashisht AA, Lin AH, Bell HN, Coppens I, Wohlschlegel JA, Bradley PJ. 2016. In Vivo Biotinylation of the Toxoplasma Parasitophorous Vacuole Reveals Novel Dense Granule Proteins Important for Parasite Growth and Pathogenesis. mBio 7:e00808-16.

25. Zhang YW, Halonen SK, Ma YF, Wittner M, Weiss LM. 2001. Initial characterization of CST1, a Toxoplasma gondii cyst wall glycoprotein. Infect Immun 69:501–507.

26. Ferreira da Silva M da F, Barbosa HS, Groß U, Lüder CGK. 2008. Stress-related and spontaneous stage differentiation of Toxoplasma gondii. Molecular BioSystems 4:824.

27. Broncel M, Treeck M. 2020. Label-Based Mass Spectrometry Approaches for Robust Quantification of the Phosphoproteome and Total Proteome in Toxoplasma gondii. Methods Mol Biol 2071:453–468.

28. Yang C, Broncel M, Dominicus C, Sampson E, Blakely WJ, Treeck M, Arrizabalaga G. 2019. A plasma membrane localized protein phosphatase in Toxoplasma gondii, PPM5C, regulates attachment to host cells. Sci Rep 9:5924.

29. Tu V, Mayoral J, Sugi T, Tomita T, Han B, Ma YF, Weiss LM. 2019. Enrichment and Proteomic Characterization of the Cyst Wall from In Vitro Toxoplasma gondii Cysts. mBio 10:e00469-19.

30. Young J, Dominicus C, Wagener J, Butterworth S, Ye X, Kelly G, Ordan M, Saunders B, Instrell R, Howell M, Stewart A, Treeck M. 2019. A CRISPR platform for targeted in

vivo screens identifies Toxoplasma gondii virulence factors in mice. 1. Nature Communications 10:1–11.

31. Braun L, Travier L, Kieffer S, Musset K, Garin J, Mercier C, Cesbron-Delauw M-F. 2008. Purification of Toxoplasma dense granule proteins reveals that they are in complexes throughout the secretory pathway. Molecular and Biochemical Parasitology 157:13–21.

32. Jones NG, Wang Q, Sibley LD. 2017. Secreted Protein Kinases Regulate Cyst Burden During Chronic Toxoplasmosis. Cell Microbiol 19.

33. Fox BA, Rommereim LM, Guevara RB, Falla A, Triana MAH, Sun Y, Bzik DJ. 2016. The Toxoplasma gondii Rhoptry Kinome Is Essential for Chronic Infection. mBio 7:e00193-16.

34. Andenmatten N, Egarter S, Jackson AJ, Jullien N, Herman J-P, Meissner M. 2013. Conditional genome engineering in Toxoplasma gondii uncovers alternative invasion mechanisms. Nat Methods 10:125–127.

35. Rommereim LM, Bellini V, Fox BA, Pètre G, Rak C, Touquet B, Aldebert D, Dubremetz J-F, Cesbron-Delauw M-F, Mercier C, Bzik DJ. 2016. Phenotypes Associated with Knockouts of Eight Dense Granule Gene Loci (GRA2-9) in Virulent Toxoplasma gondii. PLoS ONE 11:e0159306.

36. Fox BA, Falla A, Rommereim LM, Tomita T, Gigley JP, Mercier C, Cesbron-Delauw M-F, Weiss LM, Bzik DJ. 2011. Type II Toxoplasma gondii KU80 Knockout Strains Enable Functional Analysis of Genes Required for Cyst Development and Latent Infection ▽. Eukaryot Cell 10:1193–1206.

37. Donald RGK, Carter D, Ullman B, Roos DS. 1996. Insertional Tagging, Cloning, and Expression of the Toxoplasma gondii Hypoxanthine-Xanthine-Guanine Phosphoribosyltransferase Gene USE AS A SELECTABLE MARKER FOR STABLE TRANSFORMATION. J Biol Chem 271:14010–14019.

38. Ren J, Wen L, Gao X, Jin C, Xue Y, Yao X. 2009. DOG 1.0: illustrator of protein domain structures. Cell Res 19:271–273.

39. Trigg J, Gutwin K, Keating AE, Berger B. 2011. Multicoil2: predicting coiled coils and their oligomerization states from sequence in the twilight zone. PLoS ONE 6:e23519.

40. Linding R, Russell RB, Neduva V, Gibson TJ. 2003. GlobPlot: exploring protein sequences for globularity and disorder. Nucleic Acids Res 31:3701–3708.

41. Shen B, Brown KM, Lee TD, Sibley LD. 2014. Efficient Gene Disruption in Diverse Strains of Toxoplasma gondii Using CRISPR/CAS9. mBio 5:e01114-14.

42. McGovern OL, Rivera-Cuevas Y, Kannan G, Narwold AJ, Carruthers VB. 2018. Intersection of endocytic and exocytic systems in Toxoplasma gondii. Traffic 19:336–353.

43. Kafsack BFC, Beckers C, Carruthers VB. 2004. Synchronous invasion of host cells by Toxoplasma gondii. Mol Biochem Parasitol 136:309–311.

44. Cox J, Mann M. 2008. MaxQuant enables high peptide identification rates, individualized p.p.b.-range mass accuracies and proteome-wide protein quantification. Nat Biotechnol 26:1367–1372.

45. Cox J, Neuhauser N, Michalski A, Scheltema RA, Olsen JV, Mann M. 2011.

    Andromeda: a peptide search engine integrated into the MaxQuant environment. J

    Proteome Res 10:1794–1805.

46. Tyanova S, Temu T, Sinitcyn P, Carlson A, Hein MY, Geiger T, Mann M, Cox J. 2016.

    The Perseus computational platform for comprehensive analysis of (prote)omics data.

    Nat Methods 13:731–740.

Table 1. Differential phosphorylation of predicted dense granule proteins between tachyzoite and bradyzoites. Subset of Table S1 showing proteins predicted to localise to the dense granules with a Log$_2$ fold change (LFC) in protein abundance <1. LFC for proteome and the normalised LFC for each phosphosite are shown. Negative scores indicate an enrichment in bradyzoites. Full details in Table S1.

Protein ID	Protein annotation / name from ToxoDB comments		Proteome Tachy v Brady LFC
TGME49_275440	dense granule protein GRA6		-0.94
	Phosphosite positions	T v B LFC	
	112	1.45	
	118	0.98	
	128	2.12	
	132	1.94	
	133	1.23	
	134	1.38	
	218	1.74	
TGME49_213067	hypothetical protein / GRA36		-0.74
	Phosphosite positions	T v B LFC	
	67	-1.80	
	76	-1.01	
	132	-1.00	
	133	-1.03	
	171	-1.20	
TGME49_290700	hypothetical protein / GRA25		-0.68
	Phosphosite positions	T v B LFC	
	66	-1.22	
	248	1.33	
	275	1.18	
	278	1.28	
	280	1.11	
TGME49_260520	hypothetical protein / GRA53/CST6		-0.56
	Phosphosite positions	T v B LFC	
	187	-1.47	
	511	-1.91	
	513	-1.49	
TGME49_267740	hypothetical protein		-0.51
	Phosphosite positions	T v B LFC	
	195	1.67	
	196	1.08	
TGME49_312330	hypothetical protein		-0.44
	Phosphosite positions	T v B LFC	
	1790	-2.19	
	1799	-1.98	
	1801	-2.56	
	1802	-1.70	

TGME49_263220	rhoptry kinase family protein ROP21		-0.43
	Phosphosite position	T v B LFC	
	246	-1.07	
TGME49_220240	**hypothetical protein / GRA31**		**-0.42**
	Phosphosite positions	T v B LFC	
	176	1.06	
	177	1.18	
	424	1.15	
TGME49_240060	**hypothetical protein / TgIST**		**-0.41**
	Phosphosite positions	T v B LFC	
	486	1.03	
	550	1.56	
TGME49_247440	**hypothetical protein / GRA33**		**-0.37**
	Phosphosite position	T v B LFC	
	68	-0.98	
TGME49_236890	**hypothetical protein / GRA37**		**-0.33**
	Phosphosite positions	T v B LFC	
	83	-0.99	
	90	1.70	
	91	1.12	
	94	1.45	
	95	1.05	
TGME49_217680	**hypothetical protein**		**-0.30**
	Phosphosite positions	T v B LFC	
	150	-2.25	
	613	0.98	
	630	-1.33	
	632	-1.10	
	2034	-1.42	
	2039	-1.22	
TGME49_288650	**dense granule protein GRA12**		**-0.24**
	Phosphosite position	T v B LFC	
	415	-1.94	
TGME49_269690	**hypothetical protein / GRA29**		**-0.24**
	Phosphosite position	T v B LFC	
	46	-1.49	
TGME49_203310	**dense granule protein GRA7**		**-0.22**
	Phosphosite positions	T v B LFC	
	41	1.23	
	90	1.17	
	130	-1.64	
	227	1.20	
TGME49_227620	**dense granule protein GRA2**		**-0.22**
	Phosphosite positions	T v B LFC	
	56	-2.08	
	72	1.41	
	76	2.14	
TGME49_230705	**hypothetical protein / GRA51/CST3**		**-0.20**
	Phosphosite position	T v B LFC	
	72	-0.97	
TGME49_289380	**hypothetical protein / GRA39**		**-0.16**
	Phosphosite position	T v B LFC	
	326	-1.55	

TGME49_270250	dense granule protein GRA1		-0.09
	Phosphosite position	T v B LFC	
	186	-0.96	
TGME49_254720	dense granule protein GRA8		-0.01
	Phosphosite position	T v B LFC	
	198	1.10	
TGME49_200360	hypothetical protein		0.01
	Phosphosite position	T v B LFC	
	152	1.23	
TGME49_270320	protein phosphatase 2C domain-containing protein		0.02
	Phosphosite positions	T v B LFC	
	149	-1.21	
	150	-1.12	
	529	-1.38	
TGME49_311230	hypothetical protein		0.09
	Phosphosite positions	T v B LFC	
	3393	1.54	
	3456	1.27	
	3457	1.12	
	4646	1.16	
	4597	1.04	
TGME49_233010	cell-cycle-assocaited protein kinase ERK7, putative		0.12
	Phosphosite position	T v B LFC	
	631	1.14	
TGME49_201130	rhoptry kinase family protein ROP33		0.21
	Phosphosite position	T v B LFC	
	394	1.05	
TGME49_225160	hypothetical protein		0.22
	Phosphosite position	T v B LFC	
	391	-1.12	
TGME49_244530	hypothetical protein		0.24
	Phosphosite positions	T v B LFC	
	219	-1.37	
	384	-1.37	
	548	-1.21	
	552	-1.64	
TGME49_247530	hypothetical protein		0.40
	Phosphosite position	T v B LFC	
	53	1.12	
TGME49_286450	dense granule protein GRA5		0.43
	Phosphosite positions	T v B LFC	
	31	-1.63	
	33	-1.29	
	105	-1.07	
TGME49_278770	hypothetical protein		0.50
	Phosphosite positions	T v B LFC	
	220	-1.11	
TGME49_275470	dense granule protein GRA15		0.58
	Phosphosite position	T v B LFC	
	521	1.10	
TGME49_231960	omega secalin, putative / GRA28		0.65
	Phosphosite positions	T v B LFC	
	1208	1.89	

48

	1789	1.19	
TGME49_310780	**dense granule protein GRA4**		**0.65**
	Phosphosite positions	T v B LFC	
	251	-1.63	
	260	-1.62	
	278	-1.19	
	285	-1.19	
TGME49_279100	**hypothetical protein / MAF1a**		**0.71**
	Phosphosite positions	T v B LFC	
	48	-1.39	
	62	-1.20	